Bypass Decoding: A Reduced-Complexity Decoding Technique for LDPC-Coded MIMO-OFDM Systems

Yan Xin, *Member, IEEE*, Syed Aon Mujtaba, Tong Zhang, *Member, IEEE*, and Jinhua Jiang, *Student Member, IEEE*

***Abstract*—In this paper, we propose a simple reduced-complexity decoding technique called bypass decoding for low-density parity-check (LDPC)-coded multiple-input–multiple-output (MIMO) orthogonal frequency-division multiplexing (OFDM) systems. Employing the bypass decoding technique, the receiver of an LDPC-coded MIMO-OFDM system decodes a codeword in two steps based on the log-likelihood ratios (LLRs) of coded bits. The hard decisions are first made on the coded bits whose LLRs have magnitudes above a certain threshold, and the rest of the coded bits will next be decoded by using an iterative receiver. We show that, as long as the threshold is properly selected, the bypass decoding technique not only delivers considerable complexity reductions but also maintains a comparable performance in LDPC-coded MIMO-OFDM transmissions. We also provide a selection rule for choosing a suitable threshold and show its effectiveness by simulations.**

***Index Terms*—Broadband wireless communications, low-density parity-check (LDPC) codes, multiple-input–multiple-output (MIMO), orthogonal frequency-division multiplexing (OFDM), sum–product algorithm.**

I. Introduction

RECENTLY, THERE has been considerable activity toward the definition of next-generation wireless local area networks (WLANs), which are expected to offer high-speed Internet services with data rates exceeding 100 Mb/s and bring WLANs that are on par with wired Ethernet technology. However, the development of high-speed WLAN systems must cope with several challenges, such as multipath fading and interference, as well as limited transmission bandwidth and power. Recently, it has been demonstrated [1]–[7] that, for the prescribed bandwidth and power, employing multiple transmit and receive antennas [multiple-input–multiple-output (MIMO)] in an orthogonal frequency-division multiplexing (OFDM) system can considerably increase the spectral efficiency and the reliability of wireless transmissions over frequency-selective channels while minimizing equalization and symbol decoding complexity. Therefore, MIMO-OFDM offers a viable signaling technique in the design of next-generation WLANs.

To further improve the robustness as well as feasibility of MIMO-OFDM, error-correcting codes such as convolutional codes (CCs), turbo codes, or low-density parity-check (LDPC) codes must be carefully selected. Among these choices, the CC specified in the IEEE 802.11a/g standards was the most feasible solution for next-generation WLANs by examining complexity, power consumption, and cost. However, there exists a considerable power efficiency gap between the CC and the theoretical capacity limit. Recently, it has been shown in [8]–[10] that LDPC-coded MIMO-OFDM systems cannot only bridge the gap but can also provide desirable design flexibility to trade off performance against complexity. Thus, LDPC has been recently specified as an option in next-generation WLAN standards, such as IEEE 802.11n. However, the conventional iterative receiver consisting of a MIMO soft-input–soft-output (SISO) demapper (often simply called soft demapper) and an LDPC decoder suffers from increased complexity compared to a convolutional (Viterbi) receiver. It is therefore desirable to design a reduced-complexity receiver for LDPC-coded MIMO-OFDM systems.

In this paper, we propose a simple decoding technique called *bypass decoding* for LDPC-coded MIMO-OFDM systems.[1] In the proposed decoding technique, a codeword is decoded in two steps based on the log-likelihood ratios (LLRs) of the coded bits: First, the hard decisions are made on the coded bits whose LLRs have magnitudes above a certain threshold. Next, the rest of the coded bits will be decoded by using an iterative receiver that remains structurally the same as the conventional receiver but is adaptive to the number and the locations of coded bits decoded in the first step. Unlike transmissions over additive white Gaussian noise (AWGN) channels, the LLRs of an LDPC codeword in a MIMO-OFDM transmission vary with both the average (long-term) signal-to-noise ratio (SNR) and the instantaneous SNRs of the underlying subchannels (subcarriers). Intuitively, a certain fraction of coded bits transmitted through subchannels with high instantaneous SNRs can be decoded by using hard-decision decoding without incurring much performance degradation. Since these coded bits will not pass through the iterative demapping/decoding process, considerable complexity savings at each demapping/decoding iteration can be achieved. Theoretically, we have shown that,

Manuscript received May 3, 2006; revised May 31, 2007 and August 21, 2007. The review of this paper was coordinated by Dr. M. Valenti.

Y. Xin and J. Jiang are with the Department of Electrical and Computer Engineering, National University of Singapore, Singapore 117576 (e-mail: elexy@nus.edu.sg; jinhua.jiang@nus.edu.sg).

S. Aon Mujtaba is with the Wireless Systems Research Department, LSI Corporation, Allentown, PA 18109 USA (e-mail: mujtaba@lsi.com).

T. Zhang is with the Department of Electrical, Computer, and Systems Engineering, Rensselaer Polytechnic Institute, Troy, NY 12180 USA (e-mail: tzhang@ecse.rpi.edu).

Color versions of one or more of the figures in this paper are available online at http://ieeexplore.ieee.org.

Digital Object Identifier 10.1109/TVT.2007.912163

[1]The proposed decoding technique may be used in other communication systems such as code-division multiple-access systems. However, the use of OFDM facilitates the selection of the threshold, which is the key parameter in the bypass decoding algorithm.

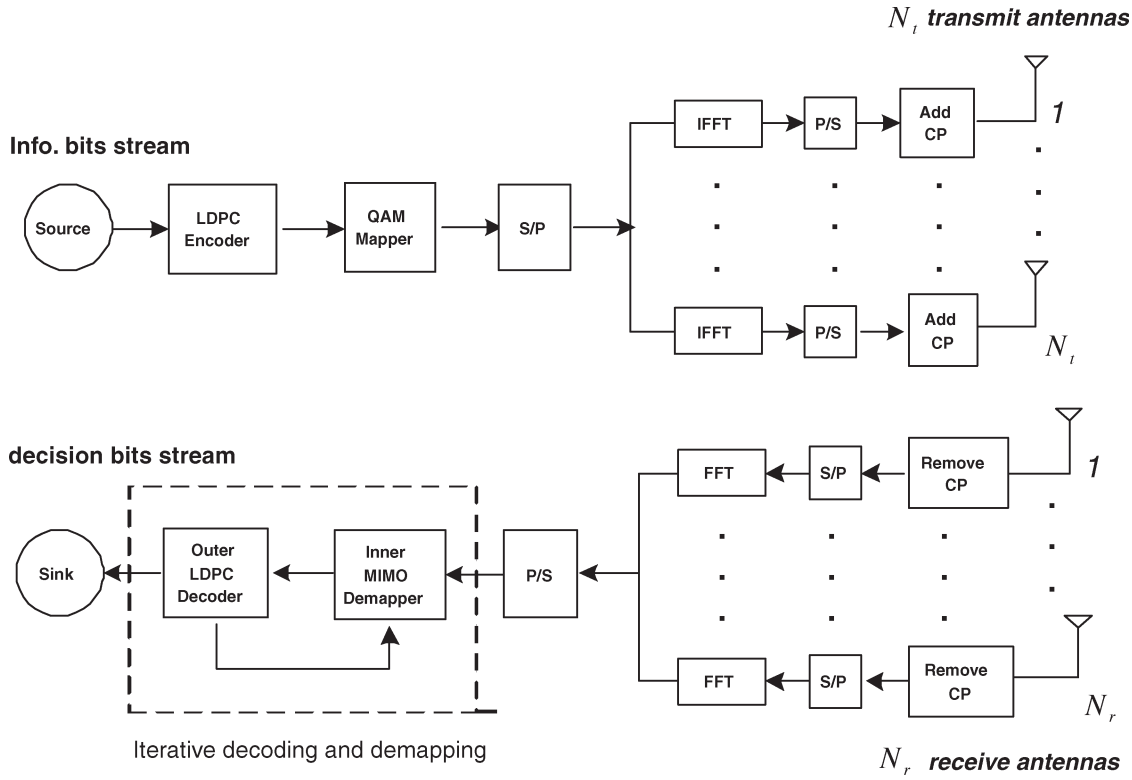

Fig. 1. LDPC-coded MIMO-OFDM system model.

in a SISO-OFDM system, using the binary phase-shift keying (BPSK) signal, for a relatively large SNR, as the threshold that is used to make hard decisions for the bits with relatively high LLRs increases, the probability of hard-decision error in decibels decreases approximately *at a constant rate*, whereas the complexity savings per demapping/decoding iteration in decibels decrease *at a rate that is inversely proportional to SNR*. Hence, it means that, for a relatively large SNR and an appropriate threshold, the probability of hard-decision error can drop to a considerably low level, whereas the complexity savings per iteration still remain significant. In more general scenarios such as MIMO-OFDM, similar phenomena can be observed through simulations. On the other hand, we have empirically shown that the number of iterations in the bypass-decoding-based iterative receiver remains almost the same as that in the conventional iterative receiver. These observations provide a rationale for adopting the bypass decoding technique for LDPC-coded MIMO-OFDM. Simulation results confirm that, compared with the conventional decoding approach, this decoding technique not only delivers a considerable reduction in decoding complexity but also maintains a comparable performance as long as a threshold is properly selected. We also provide a selection rule for choosing a suitable threshold and show its effectiveness by simulations.

The remainder of this paper is organized as follows: Section II depicts a general model for MIMO-OFDM systems, and Section III describes the conventional iterative receiver of LDPC-coded MIMO-OFDM systems. Section IV introduces the bypass decoding technique. Section V presents a method for selecting a suitable threshold. Section VI provides several simulation examples. Finally, Section VII concludes this paper.

The notations used in this paper are given as follows: Bold lower (upper) case letters are used to denote column vectors (matrices); $(\cdot)^*$ denotes the conjugate of a complex number; $(\cdot)^T$ represents the transpose of a matrix; $[\cdot]_{ij}$ denotes the (i,j)th entry of a matrix; $[\cdot]_j$ denotes the jth entry of a vector; and $\|\cdot\|$ denotes the Frobenius norm of a vector.

II. MIMO-OFDM System Model

Consider an LDPC-coded MIMO-OFDM system depicted in Fig. 1, where N_t transmit antennas, N_r receive antennas, and N_c subcarriers are used. At the transmitter, the LDPC encoder generates a sequence of codewords, each of which consists of N coded bits. Every codeword is mapped to a block of constellation symbols with size $N/\log_2|\mathcal{A}_s|$, i.e., each $\log_2|\mathcal{A}_s|$ coded bit is mapped into a constellation symbol from $\mathcal{A}_s$, where $\mathcal{A}_s$ denotes a constellation of size $|\mathcal{A}_s|$. Subsequently, the block of constellation symbols, together with the pilot symbols, is converted into N_t parallel spatial streams. The symbols in each spatial stream are parsed into N_b OFDM blocks, each containing N_c symbols. Each OFDM block is modulated by using an N_c-point inverse fast Fourier transform (FFT) and is transmitted through the corresponding antenna after a cyclic prefix (CP) insertion.

The fading channel between the ith transmit antenna and the jth receive antenna is assumed to be frequency selective and is described as $\gamma^{ji} \triangleq [\gamma_1^{ji}, \ldots, \gamma_{L+1}^{ji}]^T$, for $j = 1, \ldots, N_r$ and $i = 1, \ldots, N_t$, where $L+1$ denotes the number of the

time-domain channel taps, and each γ_l^{ji} is modeled as a zero-mean complex Gaussian random variable. We assume that 1) each γ_l^{ji} is independent of the different (i,j) pairs and is also independent of the different paths for the same (i,j) pair; 2) the average energy of γ^{ji} is assumed to be unity, i.e., $E(\|\gamma^{ji}\|^2)=1$, for all i, j; 3) the γ_l^{ji} remains invariant over a frame consisting of N_b OFDM blocks and change independently from frame to frame; and 4) perfect channel state information is available at the receiver but not at the transmitter.

At the receiver, after the removal of CP, each block at the output of each receive antenna is demodulated by using an N_c-point FFT. In particular, on the kth subcarrier, the signals $y_{k,p}^j$ of the pth OFDM block at the jth receive antenna can be expressed as $y_{k,p}^j=\sum_{i=1}^{N_t}\alpha_k^{ji}s_{k,p}^i+w_{k,p}^j$, for $k=1,\ldots,N_c$ and $p=1,\ldots,N_b$, where $s_{k,p}^i$ is the transmitted signal; $w_{k,p}^j$ denotes the AWGN with mean zero and variance σ^2, i.e., $w_{k,p}^j\sim\mathcal{CN}(0,\sigma^2)$; and α_k^{ji} is the frequency domain representation of the channel γ^{ji} from the ith transmitter to the jth receiver at the kth subcarrier. The α_k^{ji} can be expressed as $\alpha_k^{ji}=\sum_{l=1}^{L+1}\gamma_l^{ji}\exp(-2\pi\sqrt{-1}(l-1)(k-1)/N_c)$. Assumptions 1 and 2 imply that $\alpha_k^{ji}\sim\mathcal{CN}(0,1)$, and α_k^{ji} is independent of the different (j,i) pairs. We define an $N_r\times N_t$ channel matrix $\boldsymbol{A}_k$ such that $[\boldsymbol{A}_k]_{ji}\triangleq\alpha_k^{ji}$. At the kth subcarrier, after collecting the received signals from all N_r receive antennas at one symbol instant, we have

$$\boldsymbol{y}_{k,p}=\boldsymbol{A}_k\boldsymbol{s}_{k,p}+\boldsymbol{w}_{k,p} \tag{1}$$

where $\boldsymbol{y}_{k,p}$ is an $N_r\times 1$ received signal vector with $[\boldsymbol{y}_{k,p}]_j\triangleq y_{k,p}^j$, $\boldsymbol{s}_{k,p}$ is an $N_t\times 1$ transmitted signal vector with $[\boldsymbol{s}_{k,p}]_j\triangleq s_{k,p}^j$, and $\boldsymbol{w}_{k,p}$ is an $N_r\times 1$ noise vector with $[\boldsymbol{w}_{k,p}]_j\triangleq w_{k,p}^j$. With no loss of generality, we assume that codeword length N is equal to the number of coded bits within a frame, i.e., $N=N_tN_bN_d\log_2|\mathcal{A}_s|$, with N_d denoting the number of subcarriers used for transmitting data.

III. Conventional Iterative Receiver

Maximum likelihood decoding based on exhaustive search has complexity that is exponential in codeword length N and thus is practically infeasible even for a moderate N. In contrast, the iterative demapping and decoding strategy for MIMO-OFDM can achieve superior performance with much-reduced complexity, therefore receiving much attention [9], [10]. A conventional iterative receiver in an LDPC-coded MIMO-OFDM system consists of two modules (a soft demapper, and an LDPC decoder), which iteratively exchange extrinsic information to improve the system performance. Two types of the iteration processes occur in the receiver: the outer and inner iterations. The outer iteration denotes the iteration between the soft demapper and the LDPC decoder, and the inner one is the iteration within the LDPC decoder. The structure of the conventional iterative receiver can be briefly described as follows: (See [5], [9], and [11] for detailed exposition.)

Consider an LDPC codeword $\boldsymbol{c}$ with length N. According to the mapping between coded bits and constellation symbols, it can be rewritten as $\boldsymbol{c}=[\boldsymbol{c}_{1,1},\ldots,\boldsymbol{c}_{N_d,N_b}]$, where the $N_t\log_2|\mathcal{A}_s|\times 1$ vector $\boldsymbol{c}_{k,p}$ denotes the coded bits mapped into constellation symbols in $\boldsymbol{s}_{k,p}$. Without loss of generality, we consider coded bits c_l, $l=1,\ldots,N_t\log_2|\mathcal{A}_s|$ in $\boldsymbol{c}_{k,p}$ for some k and p. Let $\mathcal{M}(\cdot)$ denote the image of such a map, i.e., $\mathcal{M}(c_l)\in\boldsymbol{s}_{k,p}$. Evidently, the mapping and demapping of such coded bits c_l should be conducted at a particular kth subcarrier and pth symbol interval. However, for notational simplicity, we drop the subscripts k and p from $\boldsymbol{y}_{k,p}$, $\boldsymbol{s}_{k,p}$, and $\boldsymbol{w}_{k,p}$, as well as the subscript k from $\boldsymbol{A}_k$, and rewrite (1) as $\boldsymbol{y}=\boldsymbol{A}\boldsymbol{s}+\boldsymbol{w}$. We represent a logical one by $+1$ and a logical zero by -1. As shown in [5], [9], and [11], the LLR of the c_l output from the soft demapper is given by

$$\begin{aligned}L(c_l|\boldsymbol{y})&\triangleq\ln\frac{P(c_l=+1|\boldsymbol{y})}{P(c_l=-1|\boldsymbol{y})}\\&=L_A(c_l)\\&\quad+\ln\underbrace{\frac{\sum_{\boldsymbol{s}\in\mathcal{S}_l^+}\exp\left[-\frac{\|\boldsymbol{y}-\boldsymbol{A}\boldsymbol{s}\|^2}{\sigma^2}+\sum_{j\neq l}\frac{c_j}{2}L_A(c_j)\right]}{\sum_{\boldsymbol{s}\in\mathcal{S}_l^-}\exp\left[-\frac{\|\boldsymbol{y}-\boldsymbol{A}\boldsymbol{s}\|^2}{\sigma^2}+\sum_{j\neq l}\frac{c_j}{2}L_A(c_j)\right]}}_{L_E(c_l)}\end{aligned} \tag{2}$$

where $\mathcal{S}_l^+\triangleq\{\boldsymbol{s}:\mathcal{M}(c_l=+1)\in\boldsymbol{s}\}$, $\mathcal{S}_l^-\triangleq\{\boldsymbol{s}:\mathcal{M}(c_l=-1)\in\boldsymbol{s}\}$, $L_A(c_l)\triangleq\ln P(c_l=1)-\ln P(c_l=-1)$ denotes the extrinsic information generated from the LDPC decoder and is equal to zero at the initial outer iteration, and $L_E(c_l)$ denotes the extrinsic information computed by the soft demapper and serves as initial inputs for the inner iterative process. In each outer iteration, the soft demapper and the LDPC decoder exchange their extrinsic information. In particular, at the *initial* outer iteration, the LLR of bit c_l $L^1(c_l|\boldsymbol{y})$ is given by

$$L^1(c_l|\boldsymbol{y})=\ln\sum_{\boldsymbol{s}\in\mathcal{S}_l^+}e^{-\frac{\|\boldsymbol{y}-\boldsymbol{A}\boldsymbol{s}\|2}{\sigma^2}}-\ln\sum_{\boldsymbol{s}\in\mathcal{S}_l^-}e^{-\frac{\|\boldsymbol{y}-\boldsymbol{A}\boldsymbol{s}\|^2}{\sigma^2}}. \tag{3}$$

Using the max-log approximation [11], we can write (3) as

$$L^1(c_l|\boldsymbol{y})\approx\min_{\boldsymbol{s}\in\mathcal{S}_l^-}\|\boldsymbol{y}-\boldsymbol{A}\boldsymbol{s}\|^2\min_{\boldsymbol{s}\in\mathcal{S}_l^+}\|\boldsymbol{y}-\boldsymbol{A}\boldsymbol{s}\|^2. \tag{4}$$

The complexity of the iterative receiver consists of contributions from the soft demapper and the LDPC decoder. The maximum a posteriori (MAP) soft mapper based on exhaustive search has a complexity exponential in N_t and $|\mathcal{A}_s|$ and, thus, is not feasible in practice when either N_t or $|\mathcal{A}_s|$ is large. Extending the idea of sphere decoding (SD), Hochwald and ten Brink [11] proposed a new soft demapper that computes approximate soft information needed for the LDPC decoder with much reduced complexity. Thus, in this paper, we will mainly focus on reducing the complexity of the LDPC decoder at the algorithmic level. Among a variety of algorithms proposed for the LDPC decoder, the sum–product algorithm (SPA) attracts most attention due to its ability to attain desirable performance–complexity tradeoffs. As illustrated in Fig. 2,

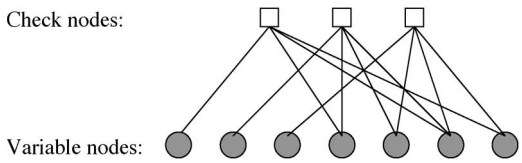

Fig. 2. Bipartite graph representation of an LDPC code.

an LDPC code can be well represented by a bipartite graph according to its parity-check matrix [12]. The top nodes of the graph are the check nodes corresponding to the parity-check equations or the rows of the parity-check matrix, whereas the bottom nodes of the graph are the variable nodes corresponding to the bits in a codeword or the columns of the parity-check matrix. In the SPA decoding, extrinsic information is exchanged along the edges between the variable nodes and check nodes in the graph (see [12] for details).

In the context of this paper, we name the conventional receiver based on the SPA as the *full SPA-based receiver*. It should be noted that the decoding complexity of an LDPC decoder depends on codeword length N, the density of the LDPC matrix $\boldsymbol{H}$, and the number of iterations used by the decoder. For example, the decoding complexity linearly grows with N for regular LDPC codes [12].

IV. Bypassed Decoding Technique

A. Motivation

As mentioned earlier, $|L^1(c_l|\boldsymbol{y})|$ is a random variable that fluctuates with both the average SNR and instantaneous SNRs of the underlying subchannels. When a coded bit is transmitted over a subchannel with a high instantaneous SNR, a hard decision based on its LLR can be made without incurring much performance degradation. In other words, depending on the average and instantaneous SNRs, certain coded bits can *bypass* the iterative demapping/decoding process, which involves most of the receiver complexity. Based on this idea, we propose the following reduced-complexity receiver for an LDPC-coded MIMO-OFDM system.

B. Two-Step Decoding

In a bypass-decoding-based iterative receiver, a codeword is decoded in two steps.

S1) *Hard-decision decoding step:* At the first outer iteration, the outputs from the soft demapper first pass through a hard-decision device based on the following decision rules:

$$\mathcal{H}_0: \quad c_l = +1, \qquad \text{if } L^1(c_l|\boldsymbol{y}) \geq +L_t \tag{5}$$

$$\mathcal{H}_1: \quad c_l = -1, \qquad \text{if } L^1(c_l|\boldsymbol{y}) \leq -L_t \tag{6}$$

where L_t denotes a threshold—a single parameter to tune tradeoffs between performance and decoding complexity. The selection of L_t will be discussed in the next section.

S2) *Iterative decoding using SPA:* After S1, certain coded bits whose $L^1(c_l|\boldsymbol{y})$ are between $-L_t$ and L_t still need to be decoded. Obviously, because some coded bits from codeword $\boldsymbol{c}$ have been decoded in S1, we need to modify the LDPC decoder to decode the rest of the coded bits. The issue of how to modify the LDPC decoder will be addressed next. The extrinsic information $L_A(c_l)$ generated from the LDPC decoder will be fed back to the demapper to update $L_E(c_l)$. Clearly, it leaves options for us to determine whether the LLRs of coded bits decoded in S1 need to be re-updated at the demapper. From the complexity perspective, we will not update the LLRs of the coded bits, which have been decoded in S1 at each outer iteration. In other words, only the coded bits whose $L^1(c_l|\boldsymbol{y})$ are between $-L_t$ and L_t will experience the iterative demapping/decoding process. By doing so, the complexity of the soft demapper is also reduced when the number of outer iterations is greater than one.

C. Modification of the LDPC Decoder

Based on the decision rules (5) and (6), the hard decisions are made on certain bits of a codeword. The locations and the number of these bits decoded in S1 vary according to the change of the average SNR and the instantaneous SNR. Hence, the LDPC decoder needs to be adaptive to the change. Suppose that a codeword $\boldsymbol{c}$ needs to be decoded. Let $\boldsymbol{H}$ be its LDPC matrix, and let $\mathcal{I}$ denote a set containing the indices of the coded bits, which have been decoded in S1. We modify the LDPC decoder in two steps.

M1) Construct a matrix $\tilde{\boldsymbol{H}}$ by removing the columns, whose column indices are in $\mathcal{I}$, from $\boldsymbol{H}$.

M2) Create a new column $\boldsymbol{h}$ by summing (binary addition) the columns whose indices belong to $\mathcal{I}_1$, which is a subset of $\mathcal{I}$ consisting of the indices of the coded bits whose value is $+1$. Concatenate $\boldsymbol{h}$ with $\tilde{\boldsymbol{H}}$ to form a new LDPC matrix denoted by $\hat{\boldsymbol{H}}$, i.e., $\hat{\boldsymbol{H}} = [\tilde{\boldsymbol{H}} \quad \boldsymbol{h}]$. This step is used to ensure that all parity-check equations are valid after the removal of the columns in step M1.

At the initial iteration, the LLRs of the undecoded bits from S1, together with the LLR (preset to be positive infinity) of an extra bit corresponding to column $\boldsymbol{h}$, are input to the modified LDPC decoder. Based on $\hat{\boldsymbol{H}}$, the modified LDPC decoder generates the extrinsic information of these bits, which is subsequently fed back to the soft demapper to proceed with the iterative process. Notice that $\boldsymbol{h}$ can be a dense column, i.e., the number of the edges, which connect the bit node corresponding to $\boldsymbol{h}$ with the check nodes in a bipartite graph [12], can be large. However, the messages along these edges do not need to be updated, because we assume that the hard-decision step is reliable.

Example 1: Consider the (7, 4) binary Hamming code with the following parity-check matrix:

$$\boldsymbol{H} = \begin{bmatrix} \mathbf{0} & 0 & \mathbf{1} & \mathbf{0} & 1 & \mathbf{1} & 1 \\ \mathbf{0} & 1 & \mathbf{0} & \mathbf{1} & 1 & \mathbf{1} & 0 \\ \mathbf{1} & 0 & \mathbf{0} & \mathbf{1} & 0 & \mathbf{1} & 1 \end{bmatrix} \rightarrow \hat{\boldsymbol{H}} = \begin{bmatrix} 0 & 1 & 1 & 1 \\ 1 & 1 & 0 & 0 \\ 0 & 0 & 1 & 1 \end{bmatrix}. \tag{7}$$

Assume that $\mathcal{I}_1 = \{1, 3\}$ and $\mathcal{I} = \{1, 3, 4, 6\}$ that includes indices corresponding to the boldface columns of $\boldsymbol{H}$. $\tilde{\boldsymbol{H}}$ can

be obtained by removing these boldface columns from $\boldsymbol{H}$. The column vector $\boldsymbol{h}$ is the sum of the first and third columns of $\boldsymbol{H}$, i.e., $\boldsymbol{h}=[1\,0\,1]^T$. We then obtain the modified parity matrix $\hat{\boldsymbol{H}}$, as shown in (7). The LLR of the bit corresponding to $\boldsymbol{h}$ is set to be positive infinity. At the first outer iteration, the LLRs corresponding to the columns of $\hat{\boldsymbol{H}}$ serve as the initial inputs to the modified LDPC decoder.

D. Implementation Considerations for the Bypass LDPC Decoder

As previously described, the bypass decoding technique requires updating the modified parity-check matrix $\hat{\boldsymbol{H}}$ according to each received codeword. From a hardware implementation perspective, a single very large scale integration (VLSI) architecture for the LDPC decoder corresponding to the parity-check matrix $\boldsymbol{H}$ is possibly essential. To be able to update the LDPC decoder, one may need to add an extra control unit at each variable node of $\boldsymbol{H}$. These control units are used to switch on or switch off variable nodes, depending on whether the input LLRs at these nodes fall in the range of $[-L_t, +L_t]$. This way of implementation is functionally equivalent to reprogramming or reconfiguring the LDPC decoder. Recently, it has been shown in [13]–[15] that a new technology using chaotic circuits is able to realize runtime reconfiguration of large-scale integrated circuits. With this development, the LDPC decoder can be potentially reconfigured at runtime; thus, the benefits of the bypass decoding technique can be achieved at the hardware implementation level.

V. Selection of a Suitable Threshold

In principle, the choice of L_t will be affected by two factors: 1) the acceptable probability of hard-decision error in S1 and 2) the affordable decoding complexity in S2. The decoding complexity in S2 depends on the average decoding codeword length (the average number of the bits in a codeword is decoded in S2) and the convergence behavior of the modified LDPC decoder. Intuitively, the larger the L_t, the lower the probability of hard-decision error in S1, the longer the average decoding codeword length, and the faster the convergence of the modified LDPC decoder. Our selection criteria is to choose such a threshold L_t in which the bypass decoding technique will offer a comparable performance to the conventional approach at a reduced complexity. Aiming at that objective, we will first examine the tradeoff between the probability of hard-decision error in step S1 and the decoding complexity in step S2.

A. Hard-Decision Error Rate versus Complexity Savings per Iteration

Let $P(\mathcal{H}_0)$ and $P(\mathcal{H}_1)$ be the *prior probabilities* of the respective hypotheses in (5) and (6). Assuming that $P(\mathcal{H}_0) = P(\mathcal{H}_1)$, the average probability of hard-decision error of bit c_l can be written as

$$P_h(e) \triangleq \frac{1}{2}\left[P\left(L^1(c_l|\boldsymbol{y}) \le -L_t|\mathcal{H}_0\right) + P\left(L^1(c_l|\boldsymbol{y}) \ge L_t|\mathcal{H}_1\right)\right]. \tag{8}$$

On the other hand, we introduce the *average* complexity saving per iteration as follows:

$$C_s \triangleq \frac{1}{2}\left[P\left(|L^1(c_l|\boldsymbol{y})| \ge L_t|\mathcal{H}_0\right) + P\left(|L^1(c_l|\mathbf{y})| \ge L_t|\mathcal{H}_1\right)\right]. \tag{9}$$

It is obvious that C_s is closely related to the *normalized* average decoding codeword length as $C_r \triangleq N_a/N = 1 - C_s$, where N_a is the average decoding codeword length in S2.

Evidently, as L_t increases, $P_h(e)$ and C_s both decrease. To quantitatively understand the convergence properties of these parameters, we start with investigating a simple case where a SISO-OFDM system with BPSK signals is considered.

1) Special Case: In a SISO-OFDM system using BPSK signals, the input–output relationship at each subcarrier can be rewritten as $y = \alpha s + w$, where $\alpha \sim \mathcal{CN}(0,1)$, $w \sim \mathcal{CN}(0,\sigma^2)$, and s is a BPSK signal. Considering s as the image of a coded bit c, i.e., $\mathcal{M}(c) = s$, the LLR of bit c at the first outer iteration is given by

$$\begin{aligned} L^1(c|y) &= \ln\frac{P(c=+1|y)}{P(c=-1|y)} = \frac{2(\alpha y^* + \alpha^* y)}{\sigma^2} \\ &= \frac{2}{\sigma^2}\left(2|\alpha|^2 s + \alpha w^* + \alpha^* w\right). \end{aligned} \tag{10}$$

Assume that $s=-1$ is transmitted. Notice that $L^1(c|y)$ is a random variable depending on both α and w, and when conditioned on $\gamma \triangleq |\alpha|^2/\sigma^2$, $L^1(c|y)$ is a real Gaussian random variable with a mean of -4γ and a variance of 8γ, i.e., $\mathcal{N}(-4\gamma, 8\gamma)$. Furthermore, γ is an exponential random variable whose probability density function (pdf) is given by [16, Tab. II]

$$p_\gamma(\gamma) \triangleq \frac{1}{\mathtt{SNR}}\exp\left(-\frac{\gamma}{\mathtt{SNR}}\right) = \sigma^2\exp(-\sigma^2\gamma), \qquad \gamma \ge 0$$

where the average SNR denoted by $\mathtt{SNR}$ is equal to $1/\sigma^2$. In addition, it can be easily verified that $P(L^1(c|y) \le -L_t|\mathcal{H}_0) = P(L^1(c|y) \ge L_t|\mathcal{H}_1)$. Thus, according to (8), the average probability of hard-decision error in S1 can be expressed as

$$\begin{aligned} P_h(e) &= P\left(L^1(c_l|y) \ge L_t|\mathcal{H}_1\right) \\ &= \sigma^2\int_0^\infty \mathcal{Q}\left(a\gamma^{-\frac{1}{2}} + b\gamma^{\frac{1}{2}}\right)e^{-\sigma^2\gamma}d\gamma \end{aligned} \tag{11}$$

where $a \triangleq L_t/\sqrt{8}$, $b \triangleq \sqrt{2}$, and $\mathcal{Q}(\cdot)$ is the complementary Gaussian cumulative distribution function defined as $\mathcal{Q}(x) \triangleq (2\pi)^{-1/2}\int_x^\infty e^{-t^2/2}dt$.

Similarly, we can obtain the average complexity saving per iteration in S2 (9) as follows:

$$C_s = \sigma^2\int_0^\infty\left[\mathcal{Q}\left(a\gamma^{-\frac{1}{2}} + b\gamma^{\frac{1}{2}}\right) + \mathcal{Q}\left(a\gamma^{-\frac{1}{2}} - b\gamma^{\frac{1}{2}}\right)\right]e^{-\sigma^2\gamma}d\gamma. \tag{12}$$

To characterize the convergence behavior of $P_h(e)$ and C_s, we introduce the so-called *decreasing rate* of these parameters.

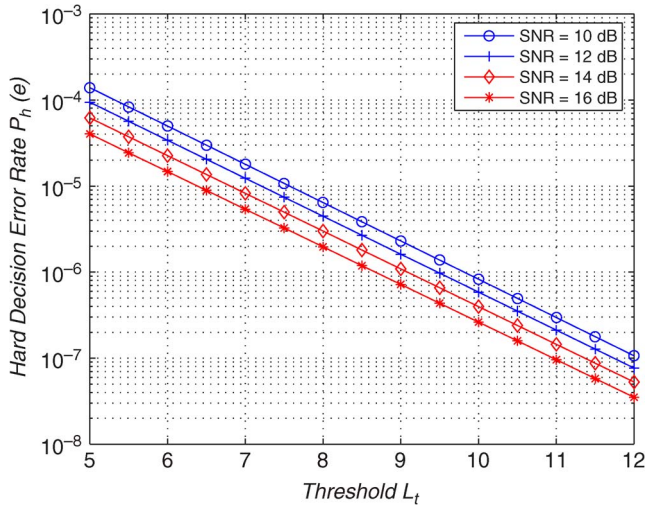

Fig. 3. Hard-decision error rate in S1 versus threshold L_t for SISO-OFDM with BPSK.

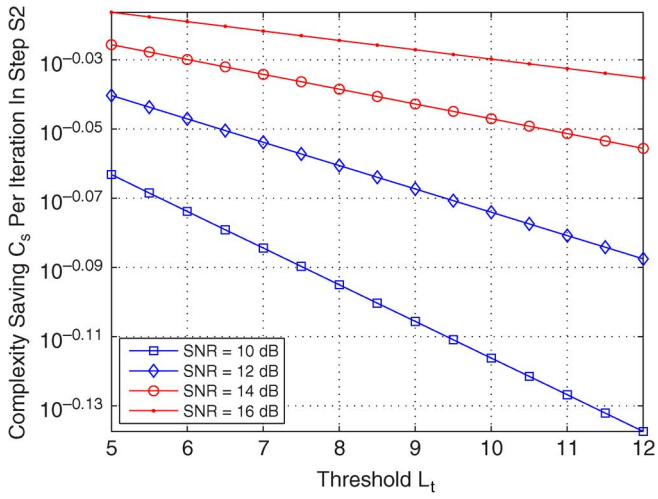

Fig. 4. Average complexity saving C_s per iteration in step S2 versus threshold L_t for SISO-OFDM with BPSK.

Definition 1: The decreasing rates of $P_h(e)$ and C_s are defined as

$$R_e \triangleq \lim_{L_t\to\infty} P_h(e)P_h(e)[\text{in decibels}]/L_t \text{ and}$$
$$R_s \triangleq \lim_{L_t\to\infty} C_s[\text{in decibels}]/L_t.$$

Basically, the decreasing rate can be used to describe how fast these two parameters decrease with L_t. Graphically, for large values of L_t, R_e and R_s are approximately equal to the slopes of the $P_h(e)$[in decibels] versus L_t and C_s[in decibels] versus L_t curves, respectively. In the following propositions, we present the results on the decreasing rates of $P_h(e)$ and C_s (see Appendices A and B, respectively, for the proofs).

Proposition 1: The decreasing rate of the probability of hard-decision error in S1 is given by

$$\begin{aligned} R_e &= \lim_{L_t\to\infty} P_h(e)[\text{in decibels}]/L_t \\ &= -10(\ln 10)^{-1} - 2.5(\ln 10)^{-1}\mathtt{SNR}^{-1} - o(\mathtt{SNR}^{-1}) \end{aligned} \quad (13)$$

where $o(\mathtt{SNR}^{-1})$ is an infinitesimal of higher order than $\mathtt{SNR}^{-1}$, i.e., $\lim_{\mathrm{SNR}\to\infty} \mathtt{SNR}\, o(\mathtt{SNR}^{-1}) = 0$.

Proposition 2: The decreasing rate of the average complexity saving per iteration in S2 is

$$\begin{aligned} R_s &= \lim_{L_t\to\infty} C_s[\text{in decibels}]/L_t \\ &= -2.5(\ln 10)^{-1}\mathtt{SNR}^{-1} - o(\mathtt{SNR}^{-1}) \end{aligned} \quad (14)$$

where $o(\mathtt{SNR}^{-1})$ is the same as that defined in Proposition 1.

According to (13), $P_h(e)$ in decibels (log scale) decreases at an almost constant rate $10(\ln 10)^{-1}$ for relatively large SNRs. Fig. 3 shows that the slopes of the curves for $\mathtt{SNR} = 10, 12, 14$, and 16 dB remain a constant, which is approximately equal to $10(\ln 10)^{-1} \approx 4.34$. Because $\mathtt{SNR} \geq 10$ dB, the value of $2.5(\ln 10)^{-1}\mathtt{SNR}^{-1} + o(\mathtt{SNR}^{-1})$ is negligible compared with $10(\ln 10)^{-1}$. On the other hand, (14) shows that, for relatively large SNRs, C_s in decibels approximately decreases in inverse proportion to SNR. Simulation results shown in Fig. 4 also validate this theoretical finding. The implication of these two propositions is that, for a relatively large L_t, as SNR increases, $P_h(e)$ becomes very small, whereas C_s remains significant.

In practice, the frame error rate (FER) serves as the major performance benchmark. We further assume that the bypass decoding will not increase the FER when the hard decisions in S1 are correct and the number of iterations is sufficiently large. Thus, the FER of the bypass-decoding-based receiver denoted by $\mathtt{FER}_{\mathrm{bypass}}$ can be upper bounded by $\mathtt{FER}_{\mathrm{bypass}} \leq \mathtt{FER}_{\mathrm{full}} + N \times P_h(e)$, where $\mathtt{FER}_{\mathrm{full}}$ denotes the FER of the full SPA receiver using only one outer iteration. For a relatively large L_t, $N \times P_h(e)$ can be used to approximate the FER incurred by hard-decision step S1. To measure the FER performance degradation due to hard-decision step S1, we introduce FER degradation factor F_d as follows:

$$F_d \triangleq \left(\mathtt{FER}_{\mathrm{full}} + N \times P_h(e)\right)/\mathtt{FER}_{\mathrm{full}}\ [\text{in decibels}]. \quad (15)$$

For convenience of illustration, we define F_d in decibels. Clearly, F_d serves as an upper bound of the ratio $\mathtt{FER}_{\mathrm{bypass}}/\mathtt{FER}_{\mathrm{Full}}$ in decibels.

Fig. 5 shows F_d versus C_s curves for different SNRs. It can be observed from Fig. 5 that the larger the SNR, the larger the complexity saving per iteration that can be obtained with the same F_d. In other words, the higher the SNR, the better the performance–complexity tradeoff. Depending on the applications, we can select an appropriate L_t. Empirically, we found that, when F_d is about 1 dB, the performance degradation is negligible, whereas the complexity saving can remain significant in this case.

2) General Cases: In MIMO-OFDM or SISO-OFDM using more general constellations, evaluating the exact pdf of $L^1(c_l|\boldsymbol{y})$ in (2) appears mathematically intractable. We next rewrite the max-log approximation of $L^1(c_l|\boldsymbol{y})$ in (4) as

$$\begin{aligned} L^1(c_l|\boldsymbol{y}) &\approx \tilde{L}^1(c_l|\boldsymbol{y}) \\ &\triangleq \frac{1}{\sigma^2}\left(\min_{\boldsymbol{s}\in\mathcal{S}_l^-}\|\boldsymbol{A}\boldsymbol{d}^- + \boldsymbol{w}\|^2 - \min_{\boldsymbol{s}\in\mathcal{S}_l^+}\|\boldsymbol{A}\boldsymbol{d}^+ + \boldsymbol{w}\|^2\right) \end{aligned} \quad (16)$$

where $\boldsymbol{d}^- \triangleq \bar{\boldsymbol{s}} - \boldsymbol{s}$ for $\boldsymbol{s} \in \mathcal{S}_l^-$, and $\boldsymbol{d}^+ \triangleq \bar{\boldsymbol{s}} - \boldsymbol{s}$ for $\boldsymbol{s} \in \mathcal{S}_l^+$, with $\bar{\boldsymbol{s}}$ denoting the actually transmitted signal. Owing to the

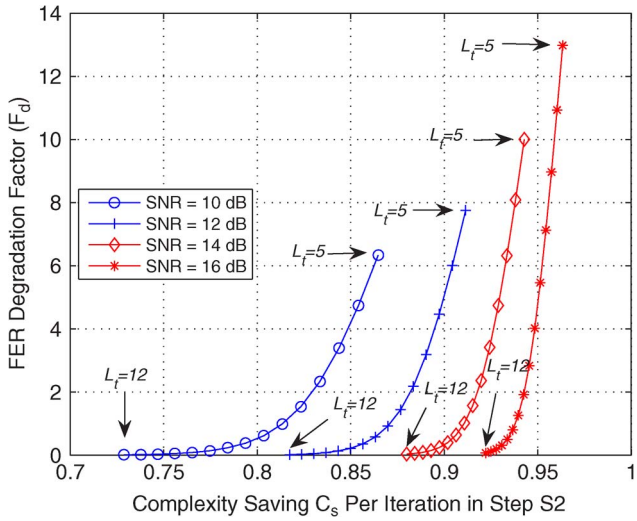

Fig. 5. FER degradation factor F_d versus average complexity savings C_s per iteration for SISO-OFDM with BPSK.

facts that the entries of $\boldsymbol{A}$ and $\boldsymbol{w}$ are independent identically distributed Gaussian random variables as well as $\boldsymbol{A}$ and $\boldsymbol{w}$ are independent, the entries of $\boldsymbol{A}\boldsymbol{d}^+ + \boldsymbol{w}$ and $\boldsymbol{A}\boldsymbol{d}^- + \boldsymbol{w}$ are complex Gaussian random variables with mean zero and respective variances $\sigma^2 + \|\boldsymbol{d}^+\|^2$ and $\sigma^2 + \|\boldsymbol{d}^-\|^2$. Thus, both $\|\boldsymbol{A}\boldsymbol{d}^+ + \boldsymbol{w}\|^2$ and $\|\boldsymbol{A}\boldsymbol{d}^- + \boldsymbol{w}\|^2$ are *Gamma* distributed with *shape* parameter N_r and respective *scale* parameters $\sigma^2 + \|\boldsymbol{d}^+\|^2$ and $\sigma^2 + \|\boldsymbol{d}^-\|^2$, i.e., $\|\boldsymbol{A}\boldsymbol{d}^+ + \boldsymbol{w}\|^2 \sim \mathcal{G}(N_r, \sigma^2 + \|\boldsymbol{d}^+\|^2)$ and $\|\boldsymbol{A}\boldsymbol{d}^- + \boldsymbol{w}\|^2 \sim \mathcal{G}(N_r, \sigma^2 + \|\boldsymbol{d}^-\|^2)$. Before presenting a guideline on the selection of L_t, we first present the following proposition to provide a rationale for us to approximate $\tilde{L}^1(c_l|\boldsymbol{y})$ (see Appendix C for the proof).

Proposition 3: Under $\mathcal{H}_1$ ($c_l = -1$ is transmitted)

$$\lim_{\lambda_d \to \infty} P\left(\|\boldsymbol{w}\|^2 = \min_{\boldsymbol{s} \in \mathcal{S}_l^-} \|\boldsymbol{A}\boldsymbol{d}^- + \boldsymbol{w}\|^2 \right) = 1$$

where $\lambda_d \triangleq d_{\min}^2/\sigma^2$, with $d_{\min}$ denoting the minimum distance between two constellation points.

Notice that λ_d is closely related to SNR defined as $N_t E_s/\sigma^2$ in the context of this paper, where E_s denotes the average symbol energy of $\mathcal{A}_s$. For example, if an M-ary square quadrature amplitude modulation (QAM) is used, E_s can be expressed in terms of $d_{\min}$ as $E_s = (M-1)d_{\min}^2/6$. Thus, Proposition 3 implies that, if we replace $\tilde{L}^1(c_l|\boldsymbol{y})$, which is given by (16), with

$$\left(\|\boldsymbol{w}\|^2 - \min_{\boldsymbol{s} \in \mathcal{S}_l^+} \|\boldsymbol{A}\boldsymbol{d}^+ + \boldsymbol{w}\|^2 \right) / \sigma^2 \tag{17}$$

the replacement does not lead to an error with high probability for a sufficiently large SNR. Hence, relying on the fact that

$$P\left(\|\boldsymbol{w}\|^2 - \min_{\boldsymbol{s} \in \mathcal{S}_l^+} \|\boldsymbol{A}\boldsymbol{d}^+ + \boldsymbol{w}\|^2 \geq L_t\sigma^2 | \mathcal{H}_1 \right)$$
$$= P\left(\min_{\boldsymbol{s} \in \mathcal{S}_l^-} \|\boldsymbol{A}\boldsymbol{d}^- + \boldsymbol{w}\|^2 - \|\boldsymbol{w}\|^2 \leq -L_t\sigma^2 | \mathcal{H}_0 \right)$$

we can approximate $P_h(e)$ in (8) as

$$P_h(e) \approx \tilde{P}_h(e) \triangleq P\left(\|\boldsymbol{w}\|^2 - \min_{\boldsymbol{s} \in \mathcal{S}_l^+} \|\boldsymbol{A}\boldsymbol{d}^+ + \boldsymbol{w}\|^2 \geq L_t\sigma^2 | \mathcal{H}_1 \right).$$

However, it is still difficult to evaluate $\tilde{P}_h(e)$, even at high SNR, because the evaluation involves computing the pdf of the order statistics of dependent random variables. Alternatively, we find a useful lower bound for $\tilde{P}_h(e)$ in the following proposition.

Proposition 4: Let V be a random variable defined as $V \triangleq X_1 - X_2$, where $X_1 \triangleq \|\boldsymbol{w}\|^2$, and $X_2 \triangleq \|\boldsymbol{A}\boldsymbol{d}_m + \boldsymbol{w}\|^2$, with $\boldsymbol{d}_m \triangleq [0, \ldots, 0, d_{\min}]^T$. Given threshold L_t, $\tilde{P}_h(e)$ can be lower bounded by

$$P_h^{\text{low}}(e) \triangleq \int_{L_t\sigma^2}^{\infty} p_V(v)dv \leq \tilde{P}_h(e) \tag{18}$$

where $p_V(v)$ denotes the pdf of random variable V.

Proof: Notice that $X_1 \sim \mathcal{G}(N_r, \sigma^2)$ and $X_2 \sim \mathcal{G}(N_r, \sigma^2 + d_{\min}^2)$. By some straightforward computations, we obtain $\text{cov}(X_1, X_2) = N_r\sigma^4$, $\text{var}(X_1) = N_r\sigma^4$, and $\text{var}(X_2) = N_r(\sigma^2 + d_{\min}^2)^2$, where $\text{cov}(\cdot)$ denotes the covariance function, and $\text{var}(\cdot)$ denotes the variance of a random variable. Hence, we can readily obtain the correlation coefficient ρ between X_1 and X_2 as $\rho = \sigma^2(\sigma^2 + d_{\min}^2)^{-1}$. Because $L_a \triangleq (\|\boldsymbol{w}\|^2 - \|\boldsymbol{A}\boldsymbol{d}_m + \boldsymbol{w}\|^2)/\sigma^2 \leq (\|\boldsymbol{w}\|^2 - \min_{\boldsymbol{s} \in \mathcal{S}_l^+} \|\boldsymbol{A}\boldsymbol{d}^+ + \boldsymbol{w}\|^2)/\sigma^2$, with $\boldsymbol{d}_m = [0, \ldots, 0, d_{\min}]^T$, we have

$$P(L_a \geq L_t | \mathcal{H}_1) \leq \tilde{P}_h(e). \tag{19}$$

Notice that $V = L_a\sigma^2 = X_1 - X_2$ is the difference of two correlated Gamma random variables. $P(L_a \geq L_t|\mathcal{H}_1)$ can be written as

$$P_h^{\text{low}}(e) \triangleq P(L_a \geq Lt | \mathcal{H}_1) = \int_{L_t\sigma^2}^{\infty} p_V(v)dv \leq \tilde{P}_h(e) \tag{20}$$

where $p_V(v)$ is given in (39). Hence, (20) concludes the proof.

Strictly speaking, (18) is a lower bound of $\tilde{P}_h(e)$, but it may not necessarily be a lower bound for $P_h(e)$, because $\tilde{P}_h(e)$ is only an approximation of $P_h(e)$. However, at high SNR, the approximation becomes quite accurate; thus, $P_h^{\text{low}}(e)$ in (18) can be used to serve as an approximation of $P_h(e)$ without incurring much error. In addition, although it is difficult to theoretically argue the accuracy of the approximation of (18), the simulation examples shown in Section VI demonstrate that (18) closely approximates $P_h(e)$, which can be used to select L_t for many cases of practical interests. Therefore, for MIMO-OFDM or SISO-OFDM using more general constellations, we adopt (18) to obtain an approximation of the FER degradation factor (15) as

$$F_d^{\text{appx}} = \left(\text{FER}_{\text{full}} + N \times P_h^{\text{low}}(e)\right) / \text{FER}_{\text{full}} \text{ [in decibels]} \tag{21}$$

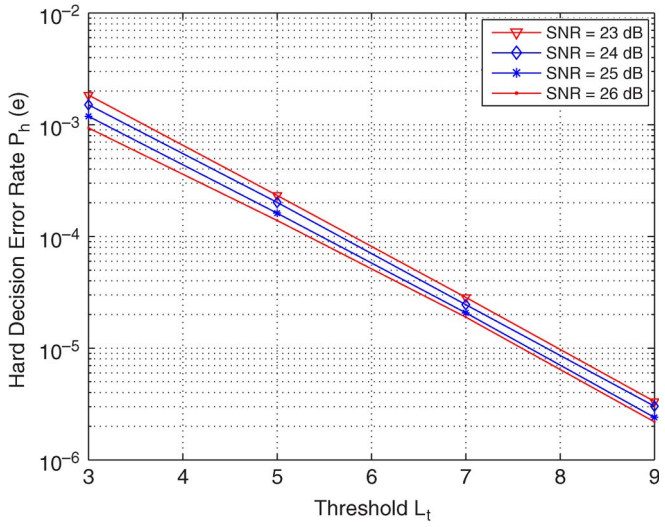

Fig. 6. Hard-decision error rate in S1 versus threshold L_t for $N_t = N_r = 2$ with 64-QAM.

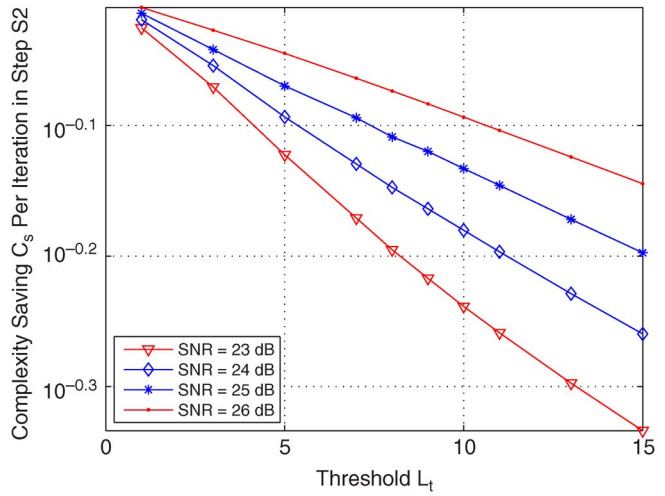

Fig. 7. Average complexity saving C_s per iteration in step S2 versus threshold L_t for $N_t = N_r = 2$ with 64-QAM.

where $P_h^{\text{low}}(e)$ in (20) can be obtained by using the *Mathematica* or *Maple* software.

In MIMO-OFDM or SISO-OFDM with more general constellations, the theoretical analysis of the convergence properties of $P_h(e)$ and C_s does not appear mathematically tractable. Empirically, we observed that, for relatively high SNR, C_s decreases at a rate inversely proportional to SNR, whereas $P_h(e)$ decreases at a constant rate that is considerably larger than the decreasing rate of C_s.

Example 2: Figs. 6 and 7 depict the convergence behavior of $P_h(e)$ and C_s as L_t increases for $N_t = N_r = 2$ with 64-QAM. Analogous to SISO-OFDM with BPSK signals, the decreasing rate of $P_h(e)$ remains as a constant for different SNRs, whereas the decreasing rate of C_s is inversely proportional to SNR. At SNR = 26 dB, F_d^{appx} is approximately 1 dB according to (21).

B. Selection Rule

Based on preceding discussions, we select L_t according to the three steps shown in Fig. 8.

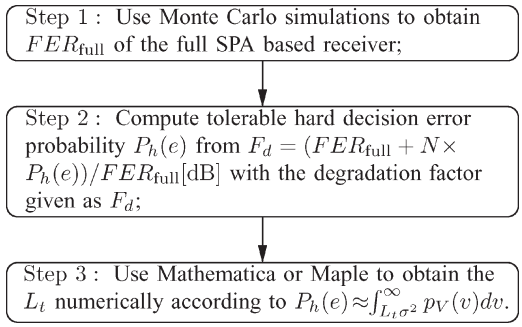

Fig. 8. Selection procedure of the threshold L_t.

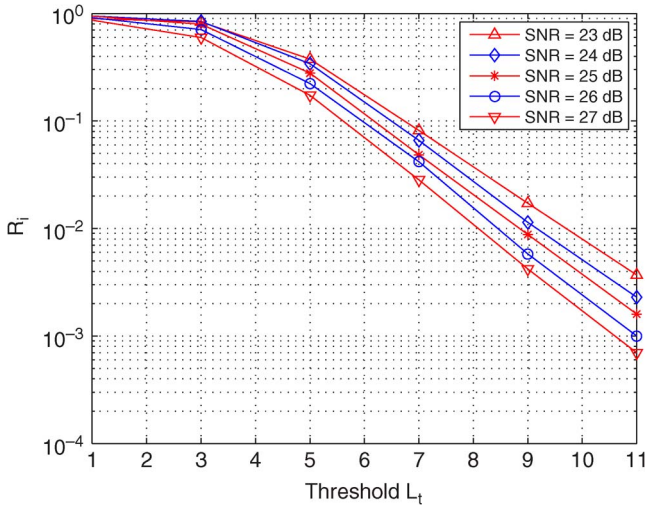

Fig. 9. Percentage of the codewords that are decoded by using different numbers of iterations in the full SPA-based and bypass-decoding-based receivers.

Regarding this threshold selection procedure, we have two remarks.

Remark 1) The FER of the full SPA-based receiver is obtained through Monte Carlo simulations.

Remark 2) Bear in mind that our design objective is to enable the bypass-decoding-based receiver to perform similarly as the full SPA-based receiver. Empirically, we found that, with F_d or F_d^{appx} about 1 dB, the bypass-decoding-based receiver can achieve considerable complexity savings with a small performance degradation.

C. The Numbers of Inner and Outer Iterations

Certainly, the number of inner iterations denoted by n^I and the number of outer iterations denoted by n^O are two other parameters that indicate the decoding complexity. The choice of the L_t has an impact on the convergence of the iterative receiver, which can be characterized by using n^I and n^O. Empirically, we observe that, with high probability, the bypass-decoding-based receiver takes exactly the same n^I and n^O to decode a codeword as the conventional receiver when we follow the aforementioned selection rule to choose L_t. To illustrate this, we provide the following simulation example.

Example 3: In Fig. 9 and Tables I–III, we use the bypass-decoding-based receiver and the full SPA receiver to decode

TABLE I
AVERAGE NUMBER OF INNER AND OUTER ITERATIONS ($N_t = N_r = 2$ WITH 64-QAM, A CODE RATE OF 3/4, $L_t = 10$, AND $n^I_{\max} = 25$)

SNR [dB]	23	24	25	26	27
n^I_{avg} (ByPass $n^O_{\max} = 1$)	6.5702	4.4376	3.0946	2.3060	1.7844
n^I_{avg} (Full SPA $n^O_{\max} = 1$)	6.5142	4.3848	3.0344	2.2265	1.6782
n^I_{avg} (ByPass $n^O_{\max} = 3$)	6.3383	5.4430	4.4497	3.5516	2.7492
n^I_{avg} (Full SPA $n^O_{\max} = 3$)	6.3186	5.4234	4.4230	3.5165	2.6962
n^O_{avg} (ByPass $n^O_{\max} = 3$)	1.7823	1.4796	1.2595	1.1361	1.0608
n^O_{avg} (Full SPA $n^O_{\max} = 3$)	1.7763	1.4738	1.2557	1.1314	1.0561

TABLE II
AVERAGE NUMBER OF INNER AND OUTER ITERATIONS ($N_t = N_r = 3$ WITH 16-QAM, A CODE RATE OF 1/2, $L_t = 10$, AND $n^I_{\max} = 15$)

SNR [dB]	13	14	15	16	17
n^I_{avg} (ByPass $n^O_{\max} = 1$)	6.9280	4.9400	3.5767	2.7620	2.1647
n^I_{avg} (Full SPA $n^O_{\max} = 1$)	6.9020	4.89867	3.5440	2.6667	2.0940
n^I_{avg} (ByPass $n^O_{\max} = 4$)	6.9575	5.0537	3.6654	3.0488	2.3916
n^I_{avg} (Full SPA $n^O_{\max} = 4$)	6.8616	4.8967	3.5423	2.6667	2.0940
n^O_{avg} (ByPass $n^O_{\max} = 4$)	1.1127	1.0313	1.0100	1.0240	1.0180
n^O_{avg} (Full SPA $n^O_{\max} = 4$)	1.1027	1.0193	1.0020	1.0000	1.0000

TABLE III
AVERAGE NUMBER OF INNER AND OUTER ITERATIONS ($N_t = N_r = 4$ WITH 4-QAM, A CODE RATE OF 1/2, $L_t = 9$, AND $n^I_{\max} = 10$)

SNR [dB]	5.5	6	6.5	7	7.5
n^I_{avg} (ByPass $n^O_{\max} = 1$)	6.3098	5.2951	4.3571	3.6436	3.1059
n^I_{avg} (Full SPA $n^O_{\max} = 1$)	6.2885	5.2392	4.3085	3.5723	3.0373
n^I_{avg} (ByPass $n^O_{\max} = 4$)	6.2599	5.4281	4.4882	3.8622	3.3327
n^I_{avg} (Full SPA $n^O_{\max} = 4$)	6.1799	5.2277	4.3104	3.5720	3.0379
n^O_{avg} (ByPass $n^O_{\max} = 4$)	1.1612	1.0846	1.0413	1.0393	1.0353
n^O_{avg} (Full SPA $n^O_{\max} = 4$)	1.1446	1.0506	1.0173	1.0040	1.0013

the same 10 000 rate-3/4 codewords (OFDM symbols) with $N = 2880$ for $N_t = N_r = 2$ with 64-QAM. In Fig. 9, the maximum number of outer iterations $n^O_{\max}$ and the maximum number of inner iterations $n^I_{\max}$ are preset to be 1 and 25, respectively. For the sake of comparison, we introduce R_i to denote the percentage of the number of the codewords that are decoded by these two receivers using different n^I's. It can be observed from Fig. 9 that, for a small L_t, R_i is quite large, whereas for $L_t = 10$ corresponding to $F_d = 1$ dB and the SNRs ranging from 23 to 27 dB, $R_i < 1\%$. In other words, over 99% of the codewords are decoded by these two receivers using exactly the same number of inner iterations. Table I lists the average number of inner iterations denoted by n^I_{avg} and the average number of outer iterations denoted by n^O_{avg} used by these two receivers to decode the same 10 000 codewords for SNRs ranging from 23 to 27 dB. It adopts the same setting as in Fig. 9, except for $n^O_{\max} = 3$ and $L_t = 10$ obtained by using the selection rule. To further validate our observation, we conduct similar comparisons for two different combinations of N_t, N_r, $n^I_{\max}$, $n^O_{\max}$, code rates, constellations, and L_t in Tables II and III. As shown in Tables I–III, there are only slight increases in n^I_{avg} and n^O_{avg} for the bypass-decoding-based receiver when L_t's are appropriately selected.

In a nutshell, empirically, we observe that, as long as an appropriate L_t is selected, the convergence of the modified iterative receiver remains roughly the same as that of the full SPA-based receiver.

D. Calculation of Total Complexity Savings

To characterize the total complexity savings by taking n_I, n_O, and the decoding length into account, we define the average *total* complexity savings for decoding a codeword as

$$T_s \triangleq \left(1 - \frac{\sum_{i=1}^{N_F} n_i^O n_i^I N_i / N_F}{N \sum_{i=1}^{N_F} n_i^O n_i^I / N_F}\right) \times 100\%$$

where N_F denotes the total number of codewords (the total number of OFDM symbols), N_i is the length of the ith codeword, and n_i^O and n_i^I denote the number of outer and inner iterations for decoding the ith codeword, respectively. In the full SPA-based receiver, $N_i = N$ for all $i = 1, \ldots, N_F$. Note that T_s does not depend on the regularity of parity-check matrices.

In step M2, computing $\boldsymbol{h}$ introduces extra complexity, because $\boldsymbol{H}$ has very low density and the operations are carried out in the binary field. At the algorithmic level, extra complexity added in M2 is much smaller compared with the complexity saved in the LDPC decoding step, which involves numerous additions in the logarithmic domain and using lookup tables [17], [18]. We thus ignore it in the calculation of T_s.

Remark: Our discussions on complexity savings remain at the algorithmic level. As discussed in Section IV, it is still perhaps necessary to use a single VLSI architecture for the LDPC decoder to support the bypass decoding algorithm at the hardware implementation level. As such, the reduced

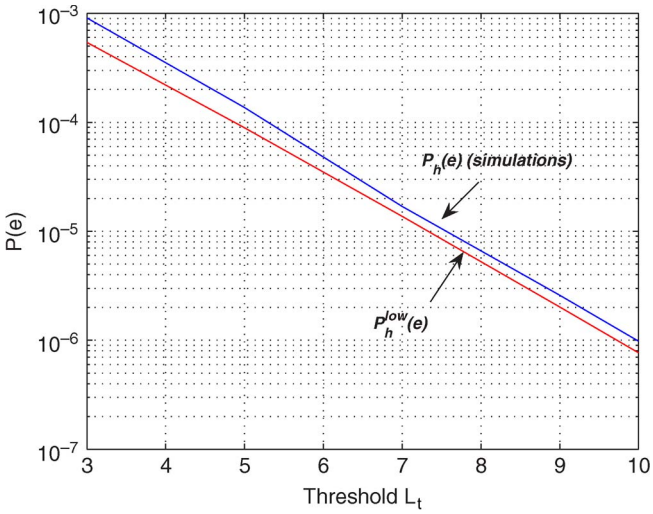

Fig. 10. Lower bound (18) versus simulated $P_h(e)$ for SNR $= 9.5$ dB, $N_t = N_r = 4$, and 4-QAM.

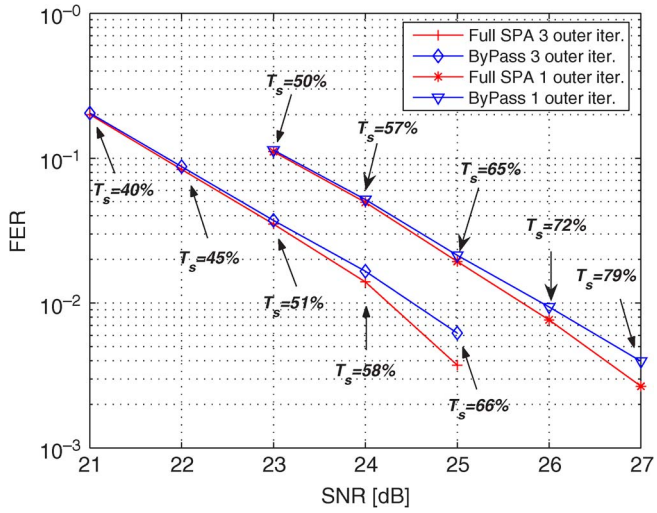

Fig. 11. FER comparisons between the full SPA-based and bypass-decoding-based receivers ($L_t = 10$ for all SNR values) for $N_t = N_r = 2$, 64-QAM, a code rate of 3/4, and $N = 2880$.

computational complexity at the algorithmic level can be potentially transferred to power reduction at the hardware level. Meanwhile, maintaining the adaptivity of the decoding architecture also consumes a certain amount of power. How to efficiently realize this transformation and attain desirable tradeoffs relies on the specific VLSI decoder architecture design and possibly further modifications of the bypassing decoding scheme. This definitely deserves further investigation, but it is beyond the scope of this paper.

VI. Simulation Results

In this section, we present several simulation examples to test the bypass decoding technique and related analysis. In all simulation examples, the channel model is chosen to be exponentially decaying multipath Rayleigh fading channels [8], i.e., $\gamma_l^{ji} = A_l^{ji}\sqrt{[1-e^{-T_s/T_{\rm rms}}]e^{-(l-1)T_s/T_{\rm rms}}}$, and $l = 1, \ldots, L+1$, where $A_l^{ji} \sim \mathcal{CN}(0,1)$, sample period T_s and the root mean square (RMS) delay spread $T_{\rm rms}$ are chosen to be 50 ns, and L is selected as 16. All the LDPC codes used in this paper are randomly generated by using the approach addressed in [19], and the column weight of these codes is chosen to be 3.

Test Case 1: Fig. 10 compares the $P_h^{\rm low}(e)$ given in (18) with the $P_h(e)$ obtained through Monte Carlo simulation for $N_t = N_r = 2$ with 64-QAM at SNR $= 26$ dB. In this figure, we use a rate-3/4 LDPC code with $N = 2880$. A similar comparison can be obtained for other configurations. As can be seen from the figure, $P_h^{\rm low}(e)$ in (18) provides a close approximation of $P_h(e)$ in both cases and is useful for selecting an appropriate L_t through the calculation of $F_d^{\rm appx}$.

Test Case 2: Fig. 11 depicts the FER performance comparisons between the full SPA-based and bypass-decoding-based receivers for $N_t = N_r = 2$ with 64-QAM. We consider two cases in Fig. 11. In the first case, $n_{\max}^O = 1$, and $n_{\max}^I = 25$, whereas in the second case, $n_{\max}^O = 3$, and $n_{\max}^I = 8$. In both cases, we use a rate-3/4 LDPC code with $N = 2880$ and select $L_t = 10$ for the bypass-decoding-based scheme, which yields $F_d^{\rm appx} \approx 1$ dB at SNR $= 26$ dB. Fig. 11 shows that, compared

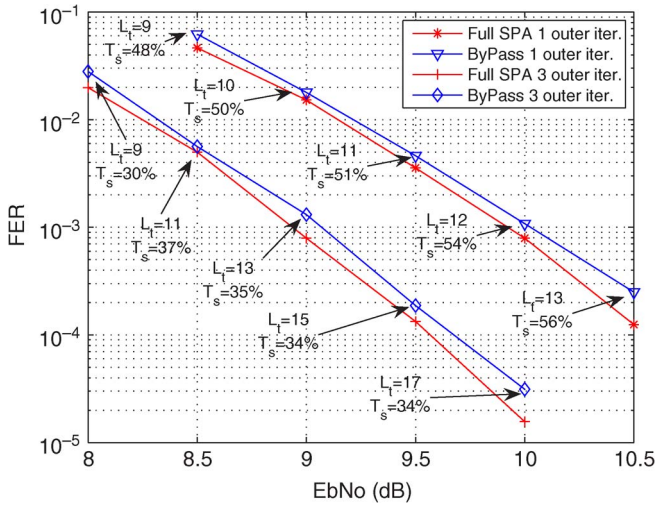

Fig. 12. FER comparisons between the full SPA-based and bypass-decoding-based receivers for $N_t = N_r = 4$, 4-QAM, a code rate of 3/4, and $N = 1920$.

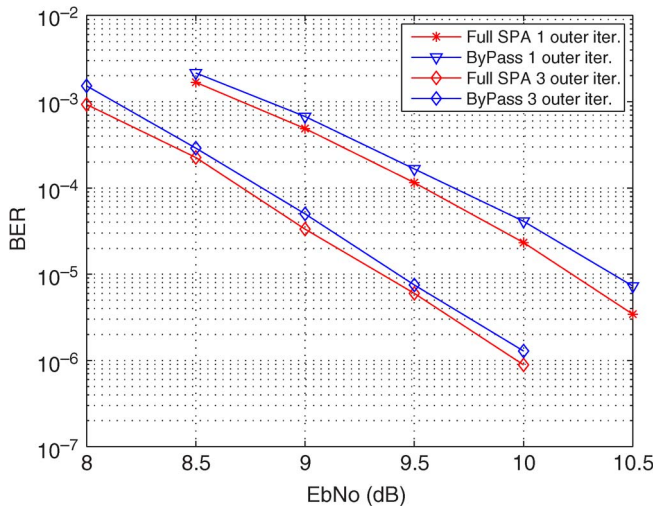

Fig. 13. BER comparisons between the full SPA-based and bypass-decoding-based receivers for $N_t = N_r = 4$, 4-QAM, a code rate of 3/4, and $N = 1920$.

TABLE IV
SELECTION OF THRESHOLD VALUES L_t FOR DIFFERENT SYSTEM PARAMETERS

Parameters	Performance Degradation	P_h^{low} or $P_h(e)$	T_s	L_t
$N_t = N_r = 1$, BPSK, 10 dB	0.16 dB	3.8×10^{-6}	59%	8.5
$N_t = N_r = 2$, 64-QAM, 24 dB	0.05 dB	1.7×10^{-7}	57%	10
$N_t = N_r = 3$, 16-QAM, 17 dB	0.18 dB	4.2×10^{-6}	52%	9

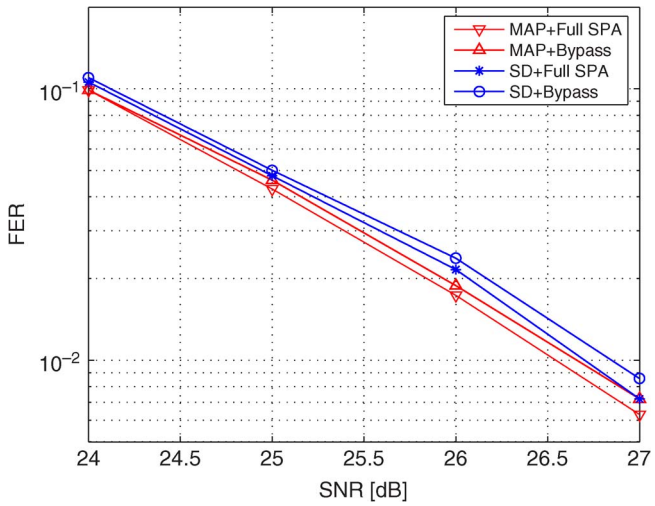

Fig. 14. FER comparisons between the MAP detector and the list-SD-based detector using the full SPA-based and bypass-decoding-based receivers for $N_t = N_r = 2$, 64-QAM, a code rate of 3/4, and $N = 2880$.

with the full SPA-based receiver, the bypass-decoding-based receiver can deliver considerable complexity reductions ($\geq 50\%$) in terms of T_s, with negligible FER performance degradations (≤ 0.5 dB) when SNR ranges from 23 to 27 dB. In addition, we also observe that, even though L_t is selected at SNR $=$ 26 dB, it also works well for different SNRs. In other words, the performance degradation is not sensitive to a variation of SNR.

Test Case 3: Figs. 12 and 13 show the FER and bit error rate (BER) comparisons for $N_t = N_r = 4$ with 4-QAM, respectively. However, in the bypass decoding scheme, we basically keep $F_d^{\text{appx}} \approx 1$ dB, which yields different L_t's at different SNRs. Still, we consider the same two cases as those in test case 2, except that we use a rate-3/4 LDPC code with $N = 1920$ and different choices of L_t. Interestingly, we observed that, for different SNRs, T_s remains roughly constant in both cases. Similar to test case 2, the bypass-decoding-based receivers can achieve more than 30% total complexity savings with a performance degradation of less than 0.2 dB.

Test Case 4: Table IV summarizes threshold values L_t for various configurations of N_t, N_r, constellations, and SNRs. The L_t's presented in the table are obtained by following the selection rule in Section V-B. By choosing $N = 2880$ and different F_d's or F_d^{appx}'s, different performance–complexity tradeoffs can be attained.

Test Case 5: Fig. 14 describes the performance comparisons among the following combinations of the detectors and decoders: the MAP detector with the full SPA- and bypass-based decoders and the list-SD-based detector with the full SPA- and bypass-based decoders. We consider the case where we select $N_t = N_r = 2$, 64-QAM, and a rate-3/4 LDPC code with $N = 2880$. We implement the list SD algorithm as described in [11]. $n_{\max}^O$ and $n_{\max}^I$ are selected to be 1 and 8, respectively, and $L_t = 10$ is selected. For the list-SD-based detector, we generate a list of candidates containing maximal 256 points to obtain the LLRs of each coded bit. In the original list SD algorithm [11], when all candidates in the list have 1 or 0 value on the same bit, a default value is assigned to this bit. When this happens, in the case where the list SD algorithm is combined with the bypass decoding algorithm, a default value of less than L_t is assigned, because the output of the bit from the detector is no longer reliable enough to bypass the iterative decoder. It can be seen from Fig. 14 that the bypass-based decoder, along with the list-SD-based detector, incurs only less-than-0.25-dB performance degradation as compared to a full SPA decoder with the list-SD-based detector. This demonstrates that the bypass decoding technique also works well with the list-SD-based detector from the performance point of view. Table V compares the complexity savings in the detection and decoding steps among the MAP detector with the full SPA decoder, the MAP detector with the bypass-based decoder, and the list-SD-based detector with the bypass-based decoder. Note that we have purposely chosen appropriate decoding radii such that the detection complexity is invariant for different SNRs. In Table V, the 98% saving of the detection complexity indicates that the ratio between the number of candidates in the decoding sphere and the total number of constellation points is merely 2%. It can be seen from the table that, in addition to the complexity savings achieved by the list SD algorithm in the detection step, the bypass decoding technique combined with the list-SD-based detector is still capable of delivering large complexity reductions in the decoding step.

VII. CONCLUSIONS

In this paper, we proposed a simple decoding technique to reduce the receiver complexity of LDPC-coded MIMO-OFDM systems. We have shown that the proposed decoding technique is capable of achieving a considerable complexity reduction without incurring much performance degradation. The desirable performance complexity tradeoffs can be attained as long as a single parameter called the threshold is properly selected. We provided a selection rule for finding a suitable threshold based on our theoretical and empirical findings. Simulation results corroborated the effectiveness of our selection method and illustrated that, in terms of performance–complexity tradeoffs, the receiver based on the proposed decoding technique compares favorably with the conventional receiver for LDPC-coded MIMO-OFDM communications.

TABLE V
COMPLEXITY SAVINGS OF THE DIFFERENT COMBINATIONS OF THE DETECTORS AND DECODERS

SNR [dB]	24		25		26		27	
Savings	Detector	Decoder	Detector	Decoder	Detector	Decoder	Detector	Decoder
MAP+Bypass	--	57%	--	65%	--	72%	--	79%
SD+Bypass	98%	54%	98%	60%	98%	65%	98%	70%

APPENDIX A
PROOF OF PROPOSITION 1

To prove the proposition, we need first introduce the following lemma.

Lemma 1:

$$\int_0^\infty e^{-\frac{a^2}{2\sin^2\theta}\gamma^{-1}-\left(\frac{b^2}{2\sin^2\theta}+\sigma^2\right)\gamma}d\gamma = \sqrt{\frac{L_t\pi}{2\sin^2\theta}}c_\theta^{-3}e^{-L_tc_\theta^2/2}\left[1+\sum_{n=1}^{\infty}(1,n)c_\theta^{-2n}/L_t^n\right] \quad (22)$$

where $c_\theta \triangleq (1+\sigma^2\sin^2\theta)^{1/4}/\sin\theta$, and the notation (ν,n) is defined as

$$(\nu,n) \triangleq (4\nu^2-1)\cdots\left(4\nu^2-(2n-1)^2\right)/(2^{2n}n!). \quad (23)$$

Proof of Lemma 1: To prove the lemma, we introduce the following integration formula [21, p. 340]:

$$\int_0^\infty x^{\nu-1}e^{-\beta x^{-1}-\delta x}dx = 2(\beta/\delta)^{\nu/2}K_\nu\left(2\sqrt{\beta\delta}\right) \quad (24)$$

where $K_\nu(x)$ denotes the modified *Bessel function* of the second kind and order ν defined in [21, p. 374]. The asymptotic expansion of $K_\nu(x)$ is given by [21, p. 380]

$$K_\nu(x) = (\pi/(2x))^{1/2}e^{-x}\left(1+\sum_{n=1}^{\infty}(\nu,n)/(2x)^n\right). \quad (25)$$

According to (24), the left-hand side of (22) can be expressed as

$$\int_0^\infty e^{-\left[\frac{a^2}{2\sin^2\theta}\gamma^{-1}+\left(\frac{b^2}{2\sin^2\theta}+\sigma^2\right)\gamma\right]}d\gamma = 2(\beta/\delta)^{1/2}K_1\left(2\sqrt{\beta\delta}\right) \quad (26)$$

where

$$2(\beta/\delta)^{1/2} = \left(\sqrt{1+\sigma^2\sin^2\theta}\right)^{-1/2}L_t/2 \quad (27)$$

$$2\sqrt{\beta\delta} = L_tc_\theta^2/2. \quad (28)$$

Furthermore, according to the asymptotic expansion of $K_\nu(x)$ given in (25), we have

$$K_1\left(2\sqrt{\beta\delta}\right) = \sqrt{\pi}(L_t)^{-1/2}c_\theta^{-1}e^{-\frac{L_tc_\theta^2}{2}}\left[1+\sum_{n=1}^{\infty}(1,n)c_\theta^{-2n}/L_t^n\right]. \quad (29)$$

The proof of the lemma is now completed by substituting (27)–(29) into (26).

Proof of Proposition 1: Applying the alternative expression of $\mathcal{Q}(x)$ function $\mathcal{Q}(x) = \pi^{-1}\int_0^{\pi/2}e^{-x^2/(2\sin^2\theta)}d\theta$, we can rewrite (11) as follows:

$$P_h(e) = \frac{\sigma^2}{\pi}\int_0^{\frac{\pi}{2}}e^{-\frac{L_t}{2\sin^2\theta}} \times\int_0^\infty e^{-\left[\frac{a^2}{2\sin^2\theta}\gamma^{-1}+\left(\frac{b^2}{2\sin^2\theta}+\sigma^2\right)\gamma\right]}d\gamma d\theta. \quad (30)$$

Furthermore, using (22) in Lemma 1, (30) can be expressed as

$$P_h(e) = \frac{\sigma^2\sqrt{L_t}}{2\sqrt{\pi}}\int_0^{\frac{\pi}{2}}\frac{c_\theta^{-3}}{\sin^2\theta}e^{\frac{-L_t}{2\sin^2\theta}}\left(1+\sqrt{1+\sigma^2\sin^2\theta}\right) \times\left(1+\sum_{n=1}^{\infty}(1,n)c_\theta^{-2}/L_t^n\right)d\theta. \quad (31)$$

It can be readily checked that $c_\theta^{-3}(\sin\theta)^{-2}\le 1$ and $c_\theta^{-2}\le 1$ for all $\theta\in[0,\pi/2]$. According to [21, p. 380], the reminder term in (25) $\sum_{n=1}^{\infty}(1,n)c_\theta^{-2n}/L_t^n = o(1)$ is an infinitesimal of higher order than a constant, i.e., $\lim_{L_t\to\infty}o(1)=0$. For a sufficiently large L_t, we have $1+\sum_{n=1}^{\infty}(\nu,n)c_\theta^{-2n}/L_t^n\le 2$ for all $\theta\in[0,\pi]$. Thus, it can be easily seen that (31) can be upper bounded by

$$P_h(e) \le \sigma^2\pi^{-1/2}\sqrt{L_t}\int_0^{\frac{\pi}{2}}e^{-\frac{L_t}{2\sin^2\theta}\left(2+\frac{\sigma^2\sin^2\theta}{2}\right)}d\theta \le \sigma^2\sqrt{L_t\pi}e^{-\frac{L_t\sigma^2}{4}}e^{-L_t}/2$$

for a sufficiently large L_t. Hence

$$\lim_{L_t\to\infty}\frac{P_h(e)[\text{dB}]}{L_t} \le -10(\ln 10)^{-1}-2.5(\ln 10)^{-1}\sigma^2 = -10(\ln 10)^{-1}-2.5(\ln 10)^{-1}\texttt{SNR}^{-1}. \quad (32)$$

On the other hand, for a large L_t, we have $1+\sum_{n=1}^{\infty}(1,n)c_\theta^{-2n}/L_t^n\ge 1/2$. Thus, (31) is lower bounded by

$$P_h(e) \ge \frac{\sigma^2\sqrt{L_t}}{4\sqrt{\pi}(1+\sigma^2)^{3/4}}e^{-\frac{L_t\left(\sigma^2+o(\sigma^2)\right)}{4}}\int_0^{\frac{\pi}{2}}e^{-\frac{L_t}{\sin^2\theta}}\sin\theta d\theta. \quad (33)$$

Applying $\csc^2\theta = 1 + \cot^2\theta$ and replacing $\cot^2\theta$ by u in [20, p. 318, eq. 3.382 (3)], we obtain

$$\begin{aligned}\int_0^{\frac{\pi}{2}} e^{-\frac{L_t}{\sin^2\theta}}\sin\theta d\theta &= \frac{e^{-L_t}}{2}\int_0^{\infty}\frac{e^{-L_t u}}{\sqrt{u}(1+u)^{3/2}}du \\ &\geq \frac{e^{-L_t}}{2}\int_0^{\infty}\frac{e^{-L_t u}}{(1+u)^2}du \\ &= e^{-\frac{L_t}{2}}W_{-1,\frac{1}{2}}(L_t) \qquad (34)\end{aligned}$$

where $W_{-1,-1/2}$ denotes the *Whittaker* function with parameters -1 and $-1/2$. For a sufficiently large L_t, we have $W_{-1,-1/2}(L_t) \geq e^{-L_t/2}(L_t)^{-1}/2$. From (34), the lower bound of $P_h(e)$ can be further expressed as

$$\begin{aligned}P_h(e) \geq \sigma^2\sqrt{L_t}(\pi)^{-1/2}(1+\sigma^2)^{-3/4} \\ \times \exp -\frac{L_t\left(\sigma^2 + o(\sigma^2)\right)}{4}e^{-L_t}(L_t)^{-1}/8\end{aligned}$$

and thus

$$\begin{aligned}\lim_{L_t\to\infty} P_h(e)[\text{dB}]/L_t \geq -10(\ln 10)^{-1} \\ - 2.5(\ln 10)^{-1}\texttt{SNR}^{-1} - o(\texttt{SNR}^{-1}). \qquad (35)\end{aligned}$$

Combining (32) and (35), we obtain

$$\begin{aligned}-o(\texttt{SNR}^{-1}) \leq \lim_{L_t\to\infty} P_h(e)[\text{dB}]/L_t \\ -10(\ln 10)^{-1} - 2.5(\ln 10)\texttt{SNR}^{-1} \leq 0. \qquad (36)\end{aligned}$$

Clearly, (36) implies that

$$\begin{aligned}\lim_{\text{SNR}\to\infty}\texttt{SNR}\Big(\lim_{L_t\to\infty} P_h(e)[\text{dB}]/L_t \\ - \left(-10(\ln 10)^{-1} - 2.5(\ln 10)^{-1}\texttt{SNR}^{-1}\right)\Big) = 0.\end{aligned}$$

Hence, we can readily conclude the proof.

Appendix B
Proof of Proposition 2

It can be seen that (12) can be lower and upper bounded as

$$\begin{aligned}\sigma_2\int_0^{\infty}\mathcal{Q}\left(a\gamma^{-\frac{1}{2}} - b\gamma^{\frac{1}{2}}\right)e^{-\sigma^2\gamma}d\gamma \leq C_s \\ \leq 2\sigma^2\int_0^{\infty}\mathcal{Q}\left(a\gamma^{-\frac{1}{2}} - b\gamma^{\frac{1}{2}}\right)e^{-\sigma^2\gamma}d\gamma. \qquad (37)\end{aligned}$$

Following the same argument in the proof of Lemma 1, we can lower bound C_s for a large L_t as follows:

$$\begin{aligned}&\sigma^2\int_0^{\infty}\mathcal{Q}\left(a\gamma^{-\frac{1}{2}} - b\gamma^{\frac{1}{2}}\right)e^{-\sigma^2\gamma}d\gamma \\ &= \int_0^{\frac{\pi}{2}} e^{\frac{L_t}{2\sin^2\theta}}\int_0^{\infty} e^{-\frac{a^2}{2\sin^2\theta}\gamma^{-1} - \left(\frac{b^2}{2\sin^2\theta}+\sigma^2\right)\gamma}d\gamma d\theta \\ &= \int_0^{\frac{\pi}{2}}\frac{\pi\sqrt{L_t}\sin\theta}{2(1+\sigma^2\sin^2\theta)^{3/4}}e^{-L_t\frac{\sqrt{1+\sigma^2\sin^2\theta}-1}{\sin^2\theta}}\left[1+o(1)\right]d\theta \\ &\geq \frac{\pi\sqrt{L_t}}{4(1+\sigma^2)^{3/4}}e^{-L_t\left(\sigma^2+o(\sigma^2)\right)}.\end{aligned}$$

Thus, we have $\lim_{L_t\to\infty} C_s[\text{in decibels}]/L_t \geq -2.5(\ln 10)^{-1} \times \texttt{SNR}^{-1} - o(\texttt{SNR}^{-1})$. On the other hand, following the similar argument in the proof of Proposition 1, we have $\lim_{L_t\to\infty} C_s[\text{in decibels}]/L_t \leq -2.5\Lambda(\ln 10)^{-1}\texttt{SNR}^{-1}$. The proof now can be concluded.

Appendix C
Proof of Proposition 3

To prove the proposition, we need to prove the following lemma first.

Lemma 2: Consider a sequence of random variables $\{X_p\}_{p=1}^P$, where $X_p \sim \mathcal{G}(\alpha, \beta_p)$, with α being a positive integer. If $0 < \beta_1 < \beta_2 \leq \cdots \leq \beta_P$ and β_1 is a fixed constant, then $\lim_{\lambda\to\infty} P(X_1 = \min\{X_1, \ldots, X_P\}) = 1$, where $\lambda \triangleq \beta_2/\beta_1$.

Proof of Lemma 2: It is equivalent to show that $\lim_{\lambda\to\infty} P(\bigcap_{p=1}^P \mathcal{A}_p) = 1$, where $\mathcal{A}_p \triangleq \{X_1 \leq X_p\}$ for $p = 1, \ldots, P$. Because

$$P\left(\cap_{p=1}^P\mathcal{A}_p\right) = 1 - P\left(\left(\cap_{p=1}^P\mathcal{A}_p\right)^c\right) \qquad (38)$$

where superscript ^{c} denotes the complement of a set. According to the DeMorgan's law, we can write $P((\cap_{p=1}^P\mathcal{A}_p)^c) = P(\cup_{p=1}^P\mathcal{A}_p^c) \leq \sum_{p=1}^P P(\mathcal{A}_p^c)$. Thus, it is sufficient to show that $\lim_{\lambda\to\infty} P(\mathcal{A}_p^c) = 0$. By definition, $P(\mathcal{A}_p^c) = P(X_1 - X_p > 0)$. To calculate $P(X_1 - X_p > 0)$, it is necessary to know the pdf of $U \triangleq X_1 - X_p$. According to [22, eq. (22a)], the difference of two correlated Gamma random variables has the pdf given by

$$\begin{aligned}p_U(u) = \frac{\sqrt{2}}{\Gamma(\alpha)\sqrt{\pi}\sqrt{c}}u^{\alpha-\frac{1}{2}}(1/d)^{\alpha-\frac{1}{2}}\exp\left(-u\sqrt{d^2-2c}/c\right) \\ \times K_{\alpha-\frac{1}{2}}(d\cdot u/c) \qquad (39)\end{aligned}$$

where $c \triangleq 2(1-\rho)\beta_1\beta_p$, $d \triangleq \sqrt{(\beta_1+\beta_p)^2 - 4\rho\beta_1\beta_p}$, and ρ denotes the correlation coefficient between X_1 and X_p. According to the definition given in (23) and the asymptotic expansion

of $K_\nu(x)$ in (25), only the first $(\alpha-1)$ terms in $K_{\alpha-1/2}$ remain nonvanished. Thus, we can write

$$K_{\alpha-\frac{1}{2}}(d\cdot u/c)=\sqrt{\pi c/(2d\cdot u)}\exp(-d\cdot u/c)\times\left[1+\sum_{i=1}^{\alpha-1}(2u)^{-i}(c/d)^i(\alpha-1/2,i)\right].$$

After some simplifications, we can express $P(U>0)$ as

$$\begin{aligned}P(U>0)&=\int_{0^+}^{\infty}p_U(u)du\\&=\int_{0^+}^{\infty}\frac{u^{\alpha-1}}{\Gamma(\alpha)d^\alpha}\exp\left(-(d+\sqrt{d^2-2c})\frac{u}{c}\right)\\&\quad\times\sum_{i=0}^{\alpha-1}\frac{\left(\alpha-\frac{1}{2},i\right)}{(2u)^i}\left(\frac{c}{d}\right)^i du.\end{aligned}\tag{40}$$

Substituting $t\triangleq(d+\sqrt{d^2-2c})u/c$ into (40), we obtain

$$\begin{aligned}P(U>0)&=\left((1-\sqrt{1-2c/d^2})/2\right)^\alpha\int_{0^+}^{\infty}\frac{t^{\alpha-1}e^{-t}}{\Gamma(\alpha)}\\&\quad\times\sum_{i=0}^{\alpha-1}(\alpha-1/2,i)2^{-i}\frac{1}{t^i}\left(1+\sqrt{1-2c/d^2}\right)^i dt.\end{aligned}$$

Noting that $\Gamma(x)=\int_0^\infty t^{x-1}e^{-t}dt$, we rewrite $P(U>0)$ as

$$\begin{aligned}P(U>0)&=\left((1-\sqrt{1-2c/d^2})/2\right)^\alpha\\&\quad\times\sum_{i=0}^{\alpha-1}(\alpha-1/2,i)2^{-i}\left(\sqrt{1-2c/d^2}\right)^i\Gamma(\alpha-i)/\Gamma(\alpha).\end{aligned}$$

Defining $\lambda_p\triangleq\beta_p/\beta_1$, we express

$$\frac{2c}{d^2}=\frac{4(1-\rho)\lambda_p^{-1}}{\left(\lambda_p^{-1}+1\right)^2-4\rho\lambda_p^{-1}},$$

$$\left((1-\sqrt{1-2c/d^2})/2\right)^\alpha=(1-\rho)^\alpha\lambda_p^{-\alpha}+o(\lambda_p^{-\alpha}).$$

Then, it can be easily checked that $\lim_{\lambda\to\infty}P(U>0)=\lim_{\lambda_p\to\infty}P(U>0)=0$. Hence, we can conclude that $\lim_{\lambda\to\infty}P\{\bigcap_{p=1}^{P}\mathcal{A}_p\}=1$.

Proof of Proposition 3: Consider a sequence of random variables $\{\|\boldsymbol{A}\boldsymbol{d}^-+\boldsymbol{w}\|^2,\boldsymbol{s}\in\mathcal{S}_l^-\}$. Under $\mathcal{H}_1$, we have $\beta_1=\sigma^2$, $\beta_2=\sigma^2+d_{\min}^2$, and $\lambda\triangleq\beta_2/\beta_1=1+d_{\min}^2/\sigma^2$, where β_1 and β_2 follows the notations in Lemma 2. According to Lemma 2, we can readily conclude the proof.

REFERENCES

[1] R. S. Blum, Y. Li, J. H. Winters, and Q. Yan, "Improved space-time coding for MIMO-OFDM wireless communications," *IEEE Trans. Commun.*, vol. 49, no. 11, pp. 1873–1878, Nov. 2001.

[2] Y. Xin and G. B. Giannakis, "High-rate space-time layered OFDM," *IEEE Commun. Lett.*, vol. 6, no. 5, pp. 187–189, May 2002.

[3] H. Bölckei, D. Gesbert, and A. J. Paulraj, "On the capacity of OFDM-based spatial multiplexing systems," *IEEE Trans. Commun.*, vol. 50, no. 2, pp. 225–234, Feb. 2002.

[4] G. Leus and M. Moonen, "Per-tone equalization for MIMO-OFDM systems," *IEEE Trans. Signal Process.*, vol. 51, no. 11, pp. 2965–2975, Nov. 2003.

[5] A. van Zelst and T. C. W. Schenk, "Implementation of a MIMO OFDM-based wireless LAN system," *IEEE Trans. Signal Process.*, vol. 52, no. 2, pp. 483–494, Feb. 2004.

[6] Y. Xin and S. A. Mujtaba, "Bypass decoding—A novel reduced complexity decoding technique for LDPC coded MIMO-OFDM systems," in *Proc. 38th Conf. Inf. Sci. Syst.*, Princeton, NJ, Mar. 17–19, 2004.

[7] Y. Xin and S. A. Mujtaba, "A hybrid decoding approach for LDPC coded MIMO-OFDM systems," in *Proc. 38th Asilomar Conf. Signals, Syst., Comput.*, Pacific Grove, CA, Nov. 7–10, 2004, pp. 1173–1177.

[8] Y. Li and J. Moon, "Increasing data rates through iterative coding and antenna diversity in OFDM-based wireless communication," in *Proc. IEEE GLOBECOM*, San Antonio, TX, Nov. 2001, pp. 3130–3133.

[9] B. Lu, G. Yue, and X. Wang, "Performance analysis and design optimization of LDPC-coded MIMO OFDM systems," *IEEE Trans. Signal Process.*, vol. 52, no. 2, pp. 348–361, Feb. 2004.

[10] H. Lee, "LDPC coded modulation MIMO OFDM transceiver: Performance comparison with map equalization," in *Proc. IEEE VTC—Spring*, Jeju, Korea, Apr. 22–25, 2007, pp. 1178–1182.

[11] B. M. Hochwald and S. ten Brink, "Achieving near-capacity on a multiple-antenna channel," *IEEE Trans. Commun.*, vol. 51, no. 3, pp. 389–399, Mar. 2003.

[12] D. Mackay, *Information Theory, Inference, and Learning Algorithms*. Cambridge, U.K.: Cambridge Univ. Press, 2003.

[13] K. Murali, S. Sinha, and W. L. Ditto, "Implementation of NOR gate by a chaotic Chua's circuit," *Int. J. Bifur. Chaos*, vol. 13, no. 9, pp. 2669–2672, 2003.

[14] K. Murali, S. Sinha, and W. L. Ditto, "Realization of the fundamental NOR gate using a chaotic circuit," *Phys. Rev. E, Stat. Phys. Plasmas Fluids Relat. Interdiscip. Top.*, vol. 68, no. 1, pp. 016 205-1–016 205-5, Jul. 2003.

[15] T. Munakata, S. Sinha, and W. L. Ditto, "Chaos computing: Implementation of fundamental logical and arithmetic operations and memory by chaotic elements," *IEEE Trans. Circuits Syst. I, Fundam. Theory Appl.*, vol. 49, no. 11, pp. 1629–1633, Nov. 2002.

[16] M. K. Simon and M. S. Alouini, "A unified approach to the performance analysis of digital communications over generalized fading channels," *Proc. IEEE*, vol. 86, no. 9, pp. 1860–1877, Sep. 1998.

[17] M. M. Mansour and N. R. Shanbhag, "High-throughput LDPC decoder," *IEEE Trans. Very Large Scale Integr. (VLSI) Syst.*, vol. 11, no. 6, pp. 976–996, Dec. 2003.

[18] Z. Wang and Z. Cui, "A memory efficient partially parallel decoder architecture for QC-LDPC codes," in *Proc. 39th Asilomar Conf. Signals, Syst., Comput.*, Pacific Grove, CA, Oct. 30–Nov. 2 2005, pp. 729–733.

[19] D. Mackay, "Good error correcting codes based on very sparse matrices," *IEEE Trans. Inf. Theory*, vol. 45, no. 2, pp. 399–431, Mar. 1999.

[20] I. S. Gradshteyn and I. M. Ryzhik, *Table of Integrals, Series, and Products*, 4th ed. San Diego, CA: Academic, 1965.

[21] Z. X. Wang and D. R. Guo, *Special Functions*. Singapore: World Scientific, 1989.

[22] H. Holm and M. S. Alouini, "Sum and difference of two squared correlated Nakagami variates in connection with the McKay distribution," *IEEE Trans. Commun.*, vol. 52, no. 8, pp. 1367–1376, Aug. 2004.

Yan Xin (S'00–M'03) received the B.E. degree in electronics engineering from Beijing University of Technology, Beijing, China, in 1992 and the M.Sc. degree in mathematics, the M.Sc. degree in electrical engineering, and the Ph.D. degree in electrical engineering from the University of Minnesota, Minneapolis, in 1998, 2000, and 2003, respectively.

Since 2004, he has been with the Department of Electrical and Computer Engineering, National University of Singapore, where he is currently an Assistant Professor. His current research interests include multiple-input multiple-output communication, network information theory, and cognitive radio.

Dr. Xin was a corecipient of the 2004 IEEE Marconi Paper Prize Award in wireless communications.

Syed Aon Mujtaba received the B.Sc. degree in electrical engineering (with honors and distinction) from Brown University, Providence, RI, and the M.S. degree and the Ph.D. degree in electrical engineering from Stanford University, Stanford, CA.

He then joined Bell Labs (Lucent Technologies), Murray Hill, NJ, as a Member of Technical Staff with the Wireless Research Laboratory, where he worked on signal processing, systems engineering, and ASIC design for the IS-95, GSM, and 3G/UMTS standards. He is the inventor of a novel modulation scheme called SSB-QPSK and a novel interference cancellation scheme for CDMA called subsymbol multiuser detection. He was the Director of Wireless Systems Architecture at Agere Systems (the microelectronics spinoff from Lucent Technologies). He also chaired the PHY subgroup of TGnSync, i.e., an industry consortium within IEEE 802.11n, working toward standardizing the next-generation of wireless LANs based on MIMO-OFDM technology. His research group developed the industry's first MIMO-OFDM prototype targeted for wireless LAN applications operating at 162Mb/s. He is currently the Director of the Wireless Systems Research Department, LSI Corporation, Allentown, PA, where he leads the development of broadband wireless transceivers for next-generation communication systems. He has published more than two dozen papers in IEEE publications and has supervised more than a dozen graduate students. He is the holder of more than a dozen patents. His research interests include the design of wireless communication systems, digital signal processing, RF systems engineering, VLSI circuit design, and microprocessor design.

Dr. Mujtaba has served on the technical review committees of IEEE ICC, VTC, and WCNC and has delivered invited talks at IEEE conferences.

Tong Zhang (S'98–M'02) received the B.S. and M.S. degrees in electrical engineering from Xian Jiaotong University, Xian, China, in 1995 and 1998, respectively, and the Ph.D. degree in electrical engineering from the University of Minnesota, Minneapolis, in 2002.

He is currently an Assistant Professor with the Department of Electrical, Computer, and Systems Engineering, Rensselaer Polytechnic Institute, Troy, NY. His current research interests include algorithm and architecture co-design for communication and data storage systems, variation-tolerant signal processing IC design, fault-tolerant system design for digital memory, and interconnect system design for hybrid CMOS/nanodevice electronic systems.

Jinhua Jiang (S'06) received the B.Eng. degree in computer engineering from the National University of Singapore, in 2004. He is currently working toward the Ph.D. degree with the Department of Electrical and Computer Engineering, National University of Singapore.

His research interests include multiuser information theory and low-density parity-check codes.